CRYSTALLINE TEXTURE OF CoCrPt FILMS ON CrMn/NiAl AND Cr/NiAl UNDERLAYER STRUCTURES

J. ZOU *, B. LU *, A.E. BAYER **, D.E. LAUGHLIN **, and D.N. LAMBETH *
*Department of Electrical and Computer Engineering, **Department of Materials Science and Engineering, Data Storage Systems Center, Carnegie Mellon University, Pittsburgh, PA 15213, jzou@ece.cmu.edu

ABSTRACT

In this study, we examine the effects of CrMn/NiAl and Cr/NiAl underlayer structures on the crystalline texture and microstructure of CoCrPt magnetic films using x-ray and electron diffraction. The former underlayer structure was found to induce better CoCrPt $(10\bar{1}0)$ texture. The stress in the CoCrPt layer was measured. The effective in-plane anisotropy energy densities of the CoCrPt films on the above two underlayers were also measured by using out-of-plane torque and Miyajima methods and the result was consistent with the texture analysis.

INTRODUCTION

The underlayer structure has significant influence on Co alloy thin film magnetic media, because it can induce a certain texture in the Co alloy layer and control the Co alloy film grain size, via grain-to-grain epitaxy. NiAl, which has the B2 crystal structure and a lattice constant very similar to Cr, was found to be an excellent underlayer material [1,2]. It can induce unicrystalline $(10\bar{1}0)$ Co texture and smaller and more uniform Co grains. Inserting an intermediate layer of Cr, Cr alloys, or other materials, between the NiAl underlayer and Co alloy magnetic layer, was found to improve the Co in-plane texture and magnetic properties [3-6].

In this paper, the CoCrPt crystalline texture and effective in-plane anisotropy energy on two underlayer structures, CrMn/NiAl and Cr/NiAl, are compared.

EXPERIMENT

All films were deposited onto glass substrates by RF diode sputtering without substrate preheating. The Ar sputtering pressure was 10 mTorr and the base pressure was about $5x10^{-7}$ Torr. Deposition was performed at a fixed AC power density of 2.3 W/cm^2. All CoCrPt and NiAl layers were 300 and 1000 Å thick, respectively. The CrMn and Cr intermediate layer thickness was varied.

The effective in-plane anisotropy energy density of the samples was measured using torque magnetometry. Film textures were examined by x-ray diffractometry and electron microscopy (TEM).

Film stress was measured by a Tencor Alpha-Step 200 general metrology profiler. As shown in Fig. 1, after the NiAl underlayer, the CrMn or Cr intermediate layer, and the CoCrPt magnetic layer were sequentially deposited, the sample was scanned on the substrate side. Then the CoCrPt layer was removed by ion milling and the sample was scanned again on the substrate side. Using the two radii of curvature of the substrate with and without the CoCrPt layer, we calculated the stress in the CoCrPt magnetic layer by using the Stoney equation. The substrates were marked to ensure that the two scans would pass approximately the same location. The samples were supported by three steel balls to eliminate the possibility of undesired sample movement during scanning.

Mat. Res. Soc. Symp. Proc. Vol. 577 © 1999 Materials Research Society

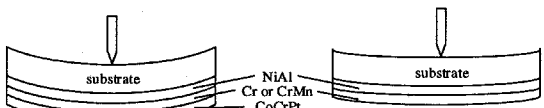

Fig. 1 Diagrammatic sketch of scanning the sample from the substrate side (a) with the CoCrPt magnetic layer and (b) with the CoCrPt layer removed.

RESULTS AND DISCUSSION

Fig. 2 shows the x-ray diffraction spectra of samples with various thicknesses of CrMn or Cr intermediate layers. Compared to the sample with no intermediate layer, adding a CrMn or Cr intermediate layer as thin as 25 Å increases the CoCrPt $(10\bar{1}0)$ peak. Further increasing the CrMn or Cr layer thickness did not improve this peak. Hence, only a very thin CrMn or Cr intermediate layer is needed to promote better in-plane texture in the CoCrPt magnetic layer. The samples with the CrMn layers showed slightly higher CoCrPt $(10\bar{1}0)$ peaks than the Cr samples with the same thickness.

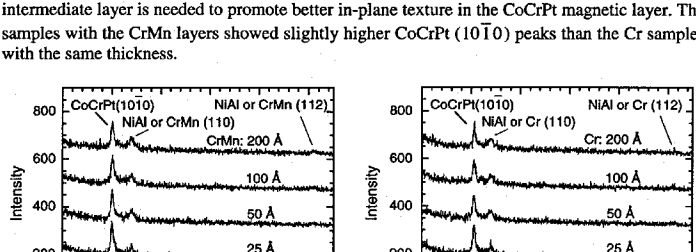

Fig. 2 X-ray spectra of (a) CoCrPt/CrMn/NiAl and (b) CoCrPt/Cr/NiAl films.

To compare the quality of the CoCrPt texture on top of the CrMn/NiAl and Cr/NiAl underlayer structures, the tilted electron diffraction technique was used [6,7]. Fig. 3 shows the 0°-tilt and 60°-tilt electron diffraction patterns of the CoCrPt layers on the above two underlayers. The CrMn and Cr intermediate layer thickness was 1000 Å. The arrows indicate the tilt axes and the three rings shown from inside to outside diameter, are $\{10\bar{1}0\}$, $\{0002\}$, and $\{10\bar{1}1\}$, respectively.

The $\{10\bar{1}0\}$ and $\{10\bar{1}1\}$ diffraction rings were present in the 0°-tilt diffraction patterns of both samples, which should not be seen in purely $(10\bar{1}0)$ textured hcp Co alloy samples. This implies that besides the $(10\bar{1}0)$ oriented CoCrPt grains, a portion of the grains were randomly oriented, for samples using both CrMn and Cr intermediate layers. This is not totally

unanticipated, as there is substantial lattice mismatch between the high Pt content Co alloy and the CrMn or the Cr intermediate layer [4]. However, the intensities of these two rings were weaker for the samples using CrMn/NiAl underlayers than for the ones using the Cr/NiAl, which indicates that CoCrPt films on the former underlayer structure have a smaller portion of randomly oriented grains than the latter one. This is unanticipated as the lattice constant of Cr is changed little by the Mn addition.

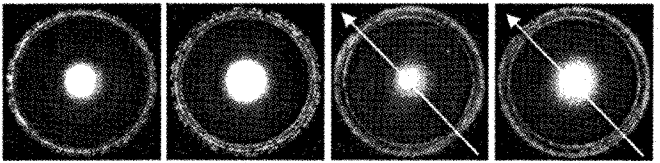

Fig. 3 The electron diffraction patterns of CoCrPt films. (a) & (c) were prepared on CrMn(1000Å)/NiAl(1000Å); (b) & (d) on Cr(1000Å)/NiAl(1000Å). (a) & (b) are 0° tilt; (c) & (d) are 60° tilt. The arrows indicate the tilt axes. The three rings shown, from inside to outside diameter, are $\{10\bar{1}0\}$, $\{0002\}$, and $\{10\bar{1}1\}$, respectively.

Tilting the sample changes the normal ring patterns into arc patterns and the length of the arcs is related to the texture axis distribution angle [6,7]. The arcs in the 60°-tilt electron diffraction pattern of the sample prepared on CrMn/NiAl underlayer structure were obviously shorter in length and more concentrated in intensity, indicating a smaller CoCrPt $(10\bar{1}0)$ texture distribution angle, than on Cr/NiAl.

Fig. 4 shows the plane-view TEM bright field images of the above two samples. The average grain size of the CoCrPt magnetic film on CrMn/NiAl underlayers was 16 nm, smaller than the 21 nm value for the sample on Cr/NiAl. The Co alloy grain size was also more evenly distributed for the former sample.

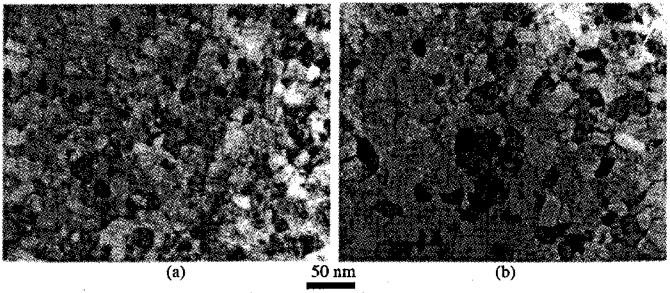

Fig. 4 Plane-view TEM bright field images of CoCrPt films on (a) CrMn(1000Å)/NiAl(1000Å) and (b) Cr(1000Å)/NiAl(1000Å) underlayers.

Fig. 5 reflects the film stress and shows the height of the sample substrate surfaces vs the scanning distance, before and after the CoCrPt magnetic layers were removed, for two samples using 1000 Å thick CrMn and Cr intermediate layers. The data points for the CoCrPt/Cr/NiAl sample in Fig. 5 (b) appear to be asymmetric, compared to the fit circle, which may be due to the substrate thickness unevenness across the scanning region. The sample using the Cr intermediate layer apparently had larger change in radius of curvature after the CoCrPt layer was removed, indicating a larger stress in the CoCrPt layer, than the sample using CrMn.

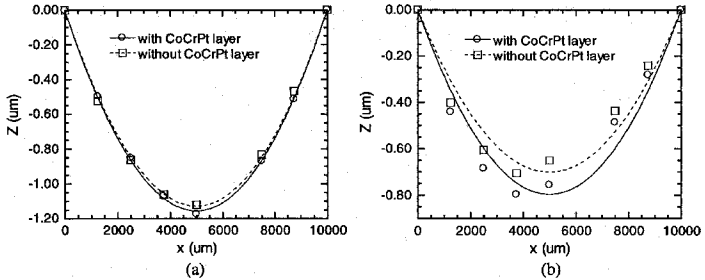

Fig. 5 The height of the substrate surface vs the scanning distance, for (a) CoCrPt/CrMn/NiAl and (b) CoCrPt/Cr/NiAl films, with and without the CoCrPt layer. The square and round dots are the experimental data and solid and dashed lines are the least squared error fit circular curves.

The stress in the CoCrPt magnetic layer was calculated using the Stoney equation:

$$\sigma = E_s d^2 (1/R - 1/R_0) / 6(1 - \nu_s)t \qquad (1)$$

where σ is the film stress, E_s and ν_s are Young's modulus and Poisson's ratio of the glass substrate, d is the substrate thickness, t is the film thickness, R and R_0 are the radii of curvature of the substrate with and without the CoCrPt layer, respectively. Table I shows the calculation results. Both samples showed compressive stress, which is consistent with the fact that Co alloys containing Pt have larger lattices than either CrMn or Cr. The CoCrPt layer had a larger compressive stress on top of the Cr/NiAl underlayers, than on the CrMn/NiAl. This is unexpected since incorporating Mn into Cr does not change the lattice constant much. However, the Mn addition into Cr may change the surface and/or the microstructure, causing the difference in the stress state in the sequentially deposited CoCrPt layer. The stress measurement results are consistent with the texture characterization – the less stressed film has the better texture.

TABLE I Stress in the CoCrPt layer for the CoCrPt/CrMn/NiAl and CoCrPt/Cr/NiAl films

Sample	R (m)	R_0 (m)	Stress (GPa)
CoCrPt/CrMn/NiAl	10.8	11.1	-0.3±0.1
CoCrPt/Cr/NiAl	15.7	17.8	-1.0±0.1

Out-of-plane torque method was used to examine the uniaxial anisotropy energy of the CoCrPt grains [8]. For a polycrystalline film with a 3D randomly distributed uniaxial crystalline anisotropy easy axes, the measured torque per unit volume by this method is:

$$L^{3D}/V = 2\pi Ms^2 \quad (2)$$

where the L^{3D} is the measured torque, V is the sample volume, and Ms is the magnetization. If the easy axes of the grains are 2D randomly distributed within the film plane, the measured torque per unit volume is:

$$L^{2D}/V = 2\pi Ms^2 + Ku/2 \quad (3)$$

where Ku is the uniaxial crystalline anisotropy energy density of the grains. We measured the out-of-plane torque using an applied magnetic field of 20 KOe, and used Eq. (3) to calculate the Ku^{eff}, which is the effective in-plane crystalline anisotropy energy density. The results are shown in Table II. The CoCrPt magnetic film had higher Ku^{eff} on CrMn/NiAl underlayers than on Cr/NiAl. This is consistent with the texture analysis results. There were more 3D randomly oriented CoCrPt grains on the Cr intermediate layer than on CrMn, which have no contribution to the Ku^{eff} obtained by this method. Furthermore, the CoCrPt $(10\bar{1}0)$ texture axis distribution angle, which is equal to the easy axis (c axis) distribution angle, was larger when prepared on Cr/NiAl than on CrMn/NiAl, giving rise to a smaller Ku^{eff} even if the crystalline anisotropy energy density of the grains was the same.

TABLE II The effective in-plane anisotropy energy density measurement results

Sample	Ku^{eff} (10^6 erg/cc)	
	Out-of-plane torque	Miyajima
CoCrPt/CrMn/NiAl	4.3	4.7
CoCrPt/Cr/NiAl	3.0	3.5

When the applied field is not much higher than the anisotropy field of the magnetic grains, the magnetization is not totally aligned with the applied field during the rotation of the sample and the out-of-plane method gives a torque value less than the ideal one when an infinitely large field is applied. Hence, this method gives the lower bound of the anisotropy energy. The Miyajima method measures 45° out-of-plane torque at a series of applied fields and the torque at the infinitely large field can be extrapolated using the equation [9,10]:

$$(L/VH)^2 = Ms^2 (L_\infty/V - L/V) / (2L_\infty/V) \quad (4)$$

where L_∞ is the torque at the infinitely large field. In Fig. 6, $(L/VH)^2$ is plotted vs L/V for both CoCrPt/CrMn/NiAl and CoCrPt/Cr/NiAl samples and the x-intercept of the extrapolated line using the high field values, gives the L_∞/V. The Ku^{eff} values calculated from L_∞/V using Eq. (3) are shown in Table II. Again, the CoCrPt film on CrMn/NiAl underlayers exhibited larger Ku^{eff} values than on Cr/NiAl.

The linear relation in Eq. (4) is strictly valid for the case that the easy axes are all aligned to one direction. For other situations such as 2D and 3D random cases, Eq. (4) is a very good approximation only when the applied field is much larger than the anisotropy field of the magnetic grains. For the field that is larger than the anisotropy field but still on the same order of magnitude, $(L/VH)^2$ is nearly a linear function of L/V, but the slope is slightly more gentle than the ideal case, causing an over-estimate of the extrapolated torque at the infinitely large field. Thus, the Miyajima method gives the upper bound of the anisotropy energy density.

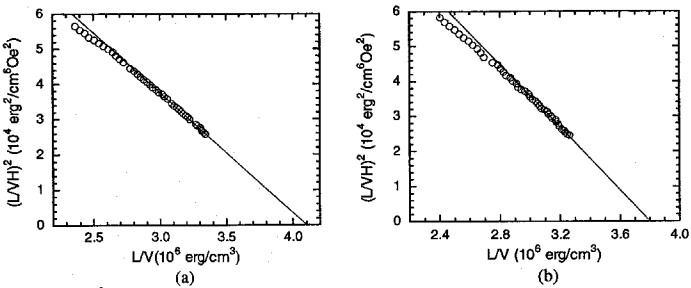

Fig. 6 $(L/VH)^2$ is plotted vs L/V for (a) CoCrPt/CrMn/NiAl and (b) CoCrPt/Cr/NiAl films.

CONCLUSIONS

Inserting a thin CrMn or Cr intermediate layer between the CoCrPt magnetic layer and the NiAl underlayer improves the CoCrPt ($10\bar{1}0$) texture. The CrMn/NiAl underlayer structure promotes better CoCrPt ($10\bar{1}0$) texture and less growth of randomly oriented CoCrPt grains than Cr/NiAl. CoCrPt films on CrMn/NiAl underlayers also have finer and more uniform grains, and less compressive stress, compared to Cr/NiAl. CoCrPt films on the former underlayer structure have higher effective in-plane anisotropy energy density, which is consistent with the texture analysis.

ACKNOWLEDGMENTS

This material is based upon the work supported in part by Seagate Technology, Inc. and by the Data Storage Systems Center of Carnegie Mellon University under a grant from the National Science Foundation # ECD-8907068. The U.S. government has certain rights to this material. A. E. Bayer was supported on an IBM Fellowship.

REFERENCES

1. L.-L. Lee, D. E. Laughlin, and D. N. Lambeth, IEEE Trans. Magn. **30**, 3951 (1994).
2. J. Li, M. Mirzamaani, X. Bian, M. Doerner, T. Arnoldussen, S. Duan, and K. Tang, to be published in J. Appl. Phys.
3. L.-L. Lee, D. E. Laughlin, L. Fang, and D. N. Lambeth, IEEE Trans. Magn. **31**, 2728 (1995).
4. J. Zou, D. E. Laughlin, and D. N. Lambeth, IEEE Trans. Magn. **34**, 1582 (1998).
5. J. Zou, D. E. Laughlin, and D. N. Lambeth, MRS Symp. Proc. **517**, 217 (1998).
6. B. Lu, D. E. Laughlin, D. N. Lambeth, S. Z. Wu, R. Ranjan, and G. C. Rauch, to be published in J. Appl. Phys.
7. L. Tang, Y. C. Feng, L.-L. Lee and D. E. Laughlin, J. Appl. Cryst. **29**, 419 (1996).
8. Y. Uesaka, K. Yoshida, Y. Nakatani, and N. Hayashi, J. Appl. Phys. **77** (10), 5303 (1995).
9. H. Miyajima and K. Sato, J. Appl. Phys. **47**, 4669 (1976).
10. H. N. Bertram and J.-G. Zhu, IEEE Trans. Magn. **27**, 5043 (1991).